# Supporting Information

# Multifunctional $Ni_3S_2$@NF-based Electrocatalysts for Efficient and Durability Electrocatalytic Water Splitting

Xiaomei Xu[a], Qiaoling Mo[b], Kuangqi Zheng[c], Zhaodi Xu[b, *], Hu Cai[a, *].

[a] School of Chemistry and Chemical Engineering, Nanchang University, 999 Xuefu Avenue, Nanchang 330031, China.

[b] Center of analysis and testing, Nanchang University, 235 Nanjing east road, Nanchang 330029, China.

[c] School of Future Technology, Nanchang University, 999 Xue fu Avenue, Nanchang 330031, China.

[*]Corresponding authors:

xuzhaodi@ncu.edu.cn (Zhaodi Xu)

caihu@ncu.edu.cn (Hu Cai)

## Experimental Section

### 1. Chemicals and Materials

Cobaltous nitrate hexahydrate (Co (NO3)2·6H2O), thiourea ($CH_4N_2S$), sodium hydroxide (NaOH), potassium hydroxide (KOH), acetone ($C_3H_6O$), hydrochloric acid (HCl,36~38%) and ethanol ($CH_3CH_2OH$, ≥99.8%) were purchased by Xilong Science Co., Ltd. Nickel nitrate hexahydrate (Ni (NO3)2·6H2O) was purchased by Tianjin Fengchuan Chemical Reagent Technology Co., Ltd. Cerium (Iii) Nitrate Hexahydrate ($CeH_{12}N_3O_{15}$) was purchased by Aladdin Chemical Reagent Company. Every chemical reagent was analytical purity.

### 2. Synthesis of $Ni_3S_2$@NF

A pretreatment of Ni foam (2 cm×3 cm) was cleaned by sonication in acetone, HCl solution (3 M), ethanol and water to remove oxides and external ions, respectively. The treated Ni foam was dried at 60 °C for 12 h under a vacuum oven. The $Ni_3S_2$@NF was prepared by a facile one-step hydrothermal method. In a typical process, 0.1 g thiourea was suspended in the mixture of water (25 mL) and ethanol (5 mL), and then the mixture was vigorously stirred for 30 min at room temperature. Subsequently, the nickel foam substrates were immersed and leaned against the wall of the autoclave and heated at 160 ℃ for 5 h. After the autoclave was cooled to room temperature naturally, the obtained $Ni_3S_2$ in situ grown on Ni foam ($Ni_3S_2$@NF) was cleaned by ethanol and deionized water several times and dried in a vacuum oven at 60 ℃ for 12 h.

### 3. Synthesis of $Ni_mCo_n$ LDH/$Ni_3S_2$@NF and $Ni_mCo_n$ LDH-$CeO_x$/$Ni_3S_2$@NF

$Ni_mCo_n$ LDH-$CeO_x$/$Ni_3S_2$@NF with different mole ratio of Ni and Co were synthesized by hydrothermal method. Firstly, mixing m mole of $Ni(NO_3)_2·6H_2O$ (m=4, 2, 1), n mole of $Co(NO_3)_3·6H_2O$ (n=1, 2, 4,)，0.5 mmol $Ce(NO_3)_2·6H_2O$ and 5 mmol hexamethylenetetramine (HMT) into 60 mL $H_2O$ to form a homogenous solution. Secondly, the above homogenous solution and $Ni_3S_2$@NF were transferred into the autoclave and heated at 160 ℃ for 6 h. Thirdly, the autoclave was cooled naturally to room temperature, and the $Ni_mCo_n$ LDH-$CeO_x$/$Ni_3S_2$@NF was

impregnated and rinsed with deionized water (DI) and dried overnight at 60 ℃. $Ni_mCo_n$ LDH/$Ni_3S_2$@NF was synthesized by the same method as utilized for $Ni_mCo_n$ LDH-$CeO_x$/$Ni_3S_2$@NF without adding $Ce(NO_3)_2 \cdot 6H_2O$. The average amount of $Ni_2Co_1$ LDH-$CeO_x$/$Ni_3S_2$@NF, $Ni_2Co_1$ LDH/$Ni_3S_2$@NF and $Ni_3S_2$@NF are 1.88, 1.78 and 0.97 $mg \cdot cm^{-2}$, respectively.

**4. Characterization**

Morphologies of the samples were probed using a HITACHI Regulus 8100 field emission scanning electron microscopy (FESEM) and JEM-2100F transmission electron microscopy (TEM). The powder X-ray diffractometer (XRD, Bruker, D8 advance, Cu Ka = 1.5406 Å, 40 kV and 40 mA) was applied to investigate the phase composition at a scan rate of 10 $° \cdot min^{-1}$. X-ray photoelectron spectroscopy (XPS, Thermo Fisher, ESCALAB 250Xi) was used to analyze the chemical state, and the binding energy of the elements was calibrated by 284.8 eV. Micro-Raman spectroscopy (Renishaw, INVIA03040430) and Infrared spectroscopy (Cary 630) were employed to analyze the functional groups of the samples.

**5. Electrochemical Measurements**

All electrochemical tests were carried out on an electrochemical workstation (CS350M) in a three-electrode system, which used as-prepared samples as the working electrodes, carbon rod as the counter electrodes and Hg/HgO as the reference electrodes. All potentials used in this study were calibrated with the Reversible Hydrogen Electrode (RHE) with the following equation: $E_{RHE} = E_{SCE} + 0.098 + 0.059$ pH, where $E_{RHE}$ was the potential versus RHE, and $E_{SCE}$ was the measured potential against the saturated Hg/HgO reference electrode. The overpotential (η) was examined to a reversible hydrogen electrode ($\eta = E_{RHE} - 1.23$ V). All the above electrochemical curves were corrected with no iR compensation. Before the OER reaction, the 1.0 M KOH electrolyte was bubbled with $N_2$ for at least 20 min to remove $O_2$. And the $N_2$ gas was purged into electrolytes before HER measurement to eliminate dissolved oxygen. The OER and HER polarization curves were recorded at a scan rate of 5.0 mV $s^{-1}$ in 1.0 M KOH electrolyte. The Tafel slopes were obtained by

analyzing the polarization curves at 5.0 $mV \cdot s^{-1}$. Electrochemical impedance spectroscopy (EIS) was carried out at -1.20 V vs. RHE and 1.24 V vs. RHE with a frequency range from 100 kHz to 0.01 Hz. The durability of the $Ni_2Co_1$ LDH-$CeO_x/Ni_3S_2$@NF was evaluated by performing a long-term controlled potential electrolysis at 100 mA for 50 h and a galvanostatic method at the current density of 100 $mA \cdot cm^{-2}$ in 1.0 M KOH electrolyte. Cyclic voltammetry (CV) curves were tested at different scan rates in the non-faradic potentials region of 0.391-0.491 V vs. RHE and -0.05-0.05V vs. RHE to determine the double-layer capacitance ($C_{dl}$) values, which was analyzing the slope of the linear fit by changing the different scan rate and then observe the corresponding current.[1]The electrochemical surface area (ECSA) was estimated according to the following equation: $ECSA=C_{dl}/C_S$, where $C_S$ is the ideal specific capacitance of the sample ($C_S = 0.040\ mF \cdot cm^{-2}$).[2]

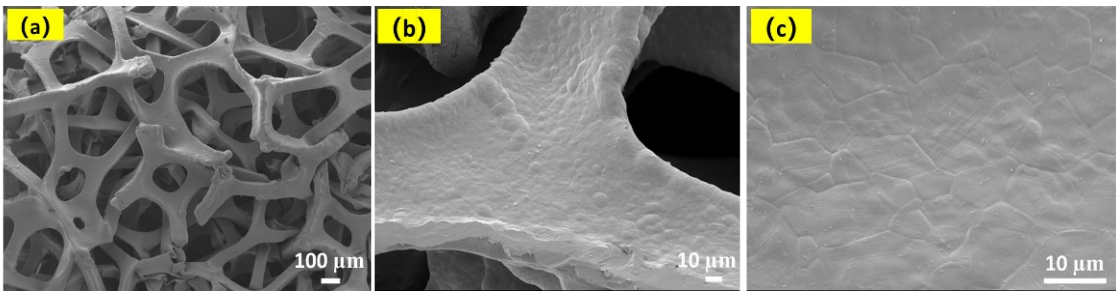


Figure S1. (a-c) SEM images of pure NF at different magnifications.

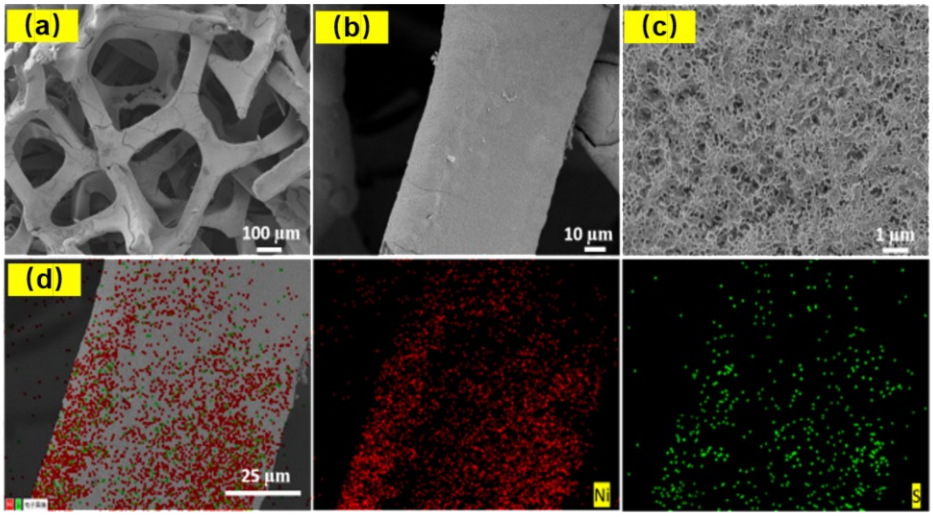


Figure S2. (a-c) SEM images of $Ni_3S_2$/NF at different magnifications, (d) SEM images of $Ni_3S_2$/NF with corresponding Ni and S elemental mapping.

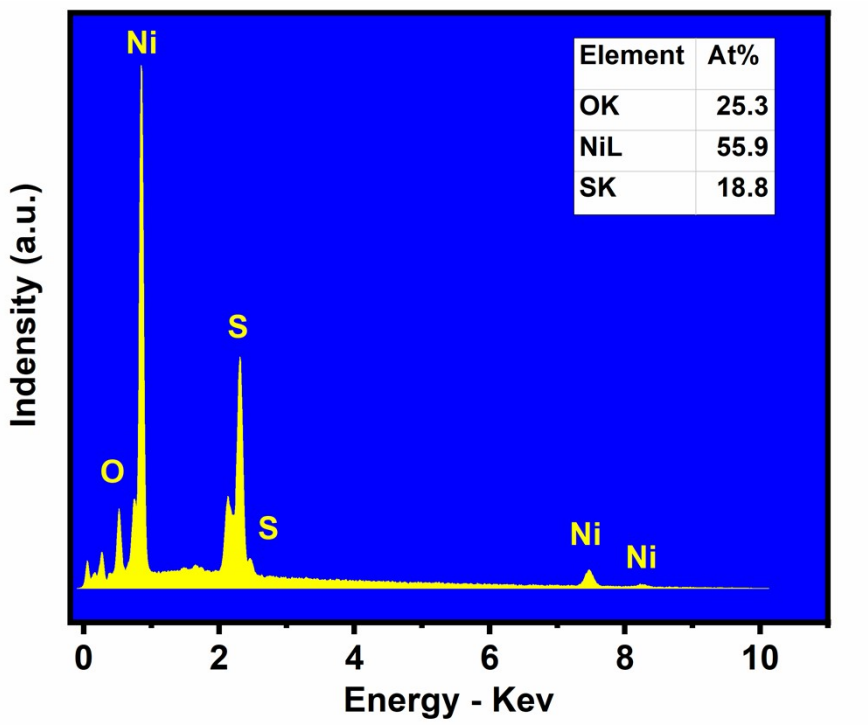


Figure S3. EDS image of $Ni_3S_2$@NF.

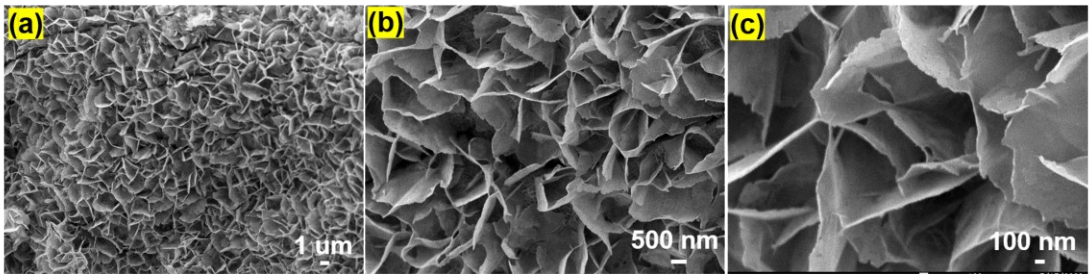

Figure S4. SEM images of $Ni_2Co_1$ LDH/$Ni_3S_2$@NF at different magnifications.

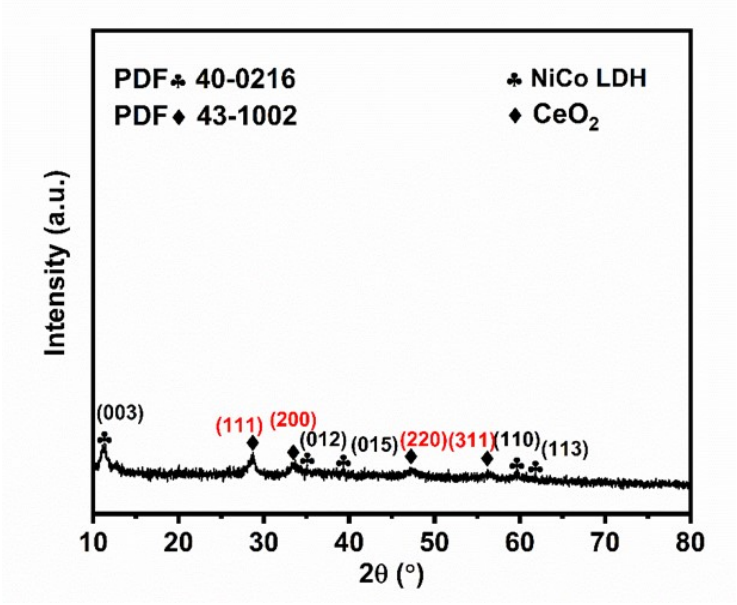


Figure S5. XRD patterns of the $Ni_2Co_1$ LDH-$CeO_x$ grown on the carbon cloth substrate.

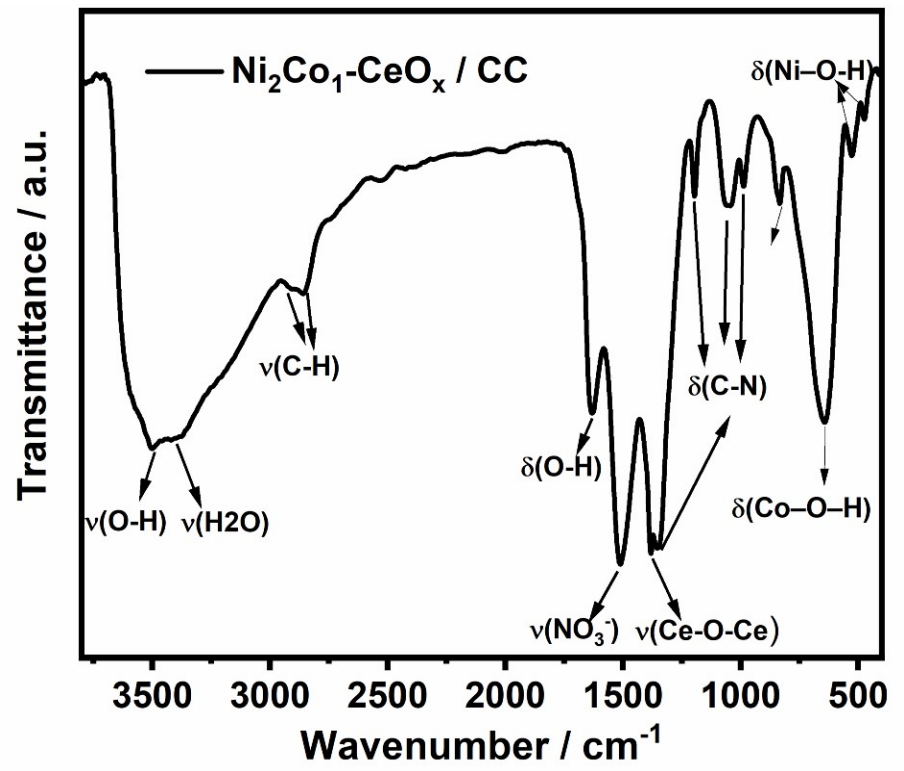


Figure S6. FT-IR spectra of $Ni_2Co_1$ LDH-$CeO_x$/CC sample.

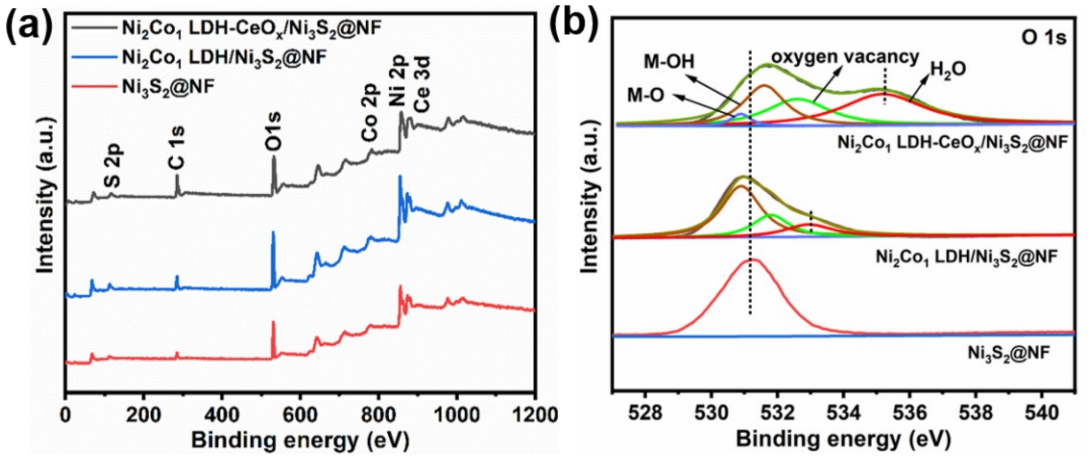


Figure S7. (a) The survey XPS spectra of $Ni_2Co_1$ LDH-$CeO_x$/$Ni_3S_2$@NF, $Ni_2Co_1$ LDH/$Ni_3S_2$@NF, and $Ni_3S_2$@NF. (b) High-resolution XPS spectra of O 1s of $Ni_2Co_1$LDH-$CeO_x$/$Ni_3S_2$@NF, $Ni_2Co_1$ LDH /$Ni_3S_2$@NF and $Ni_3S_2$@NF.

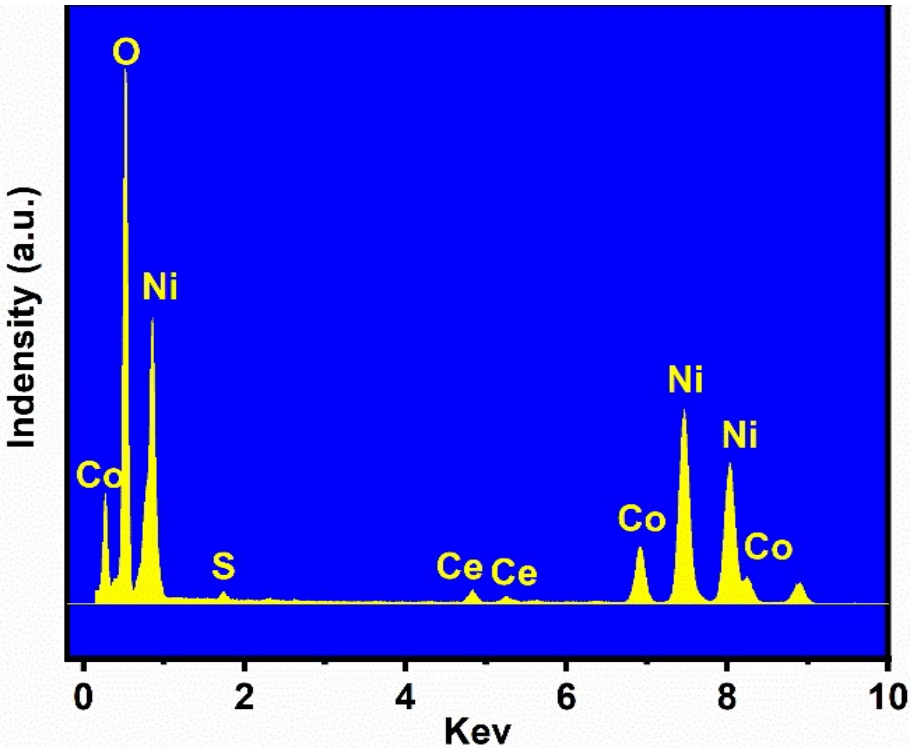


Figure S8. EDS image of $Ni_2Co_1$ LDH-$CeO_x$/$Ni_3S_2$@NF.

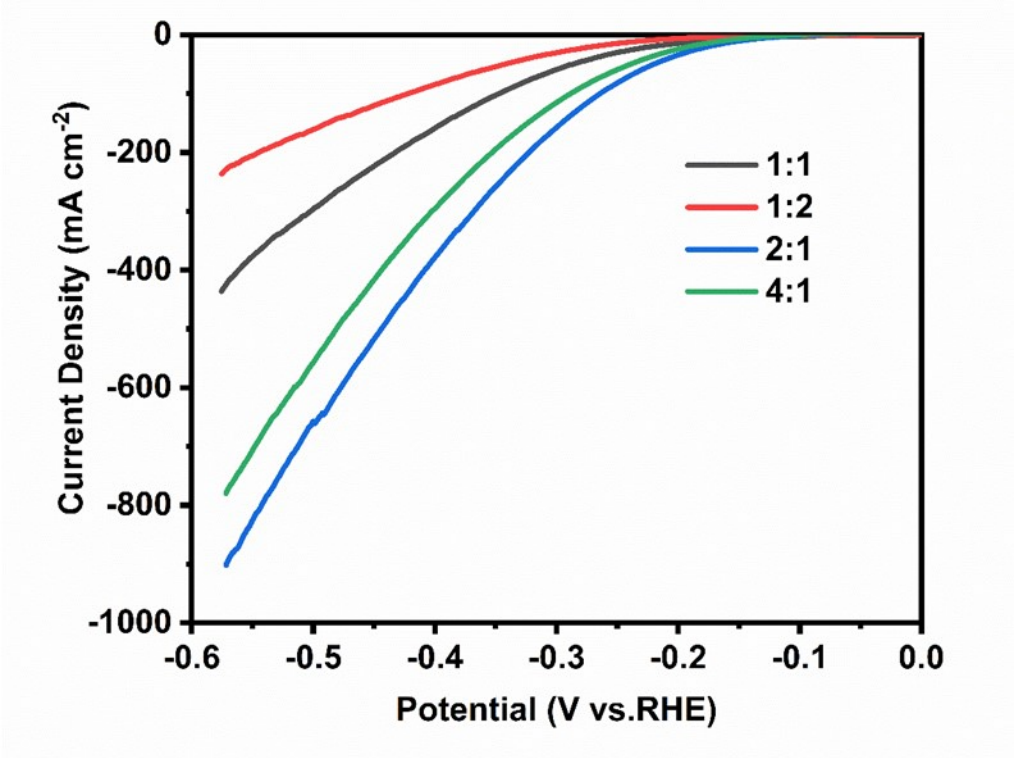


Figure S9. LSV curves of $Ni_mCo_n$ LDH-$CeO_x$/$Ni_3S_2$@NF prepared at different Ni/Co feeding ratios for HER in 1 M KOH.

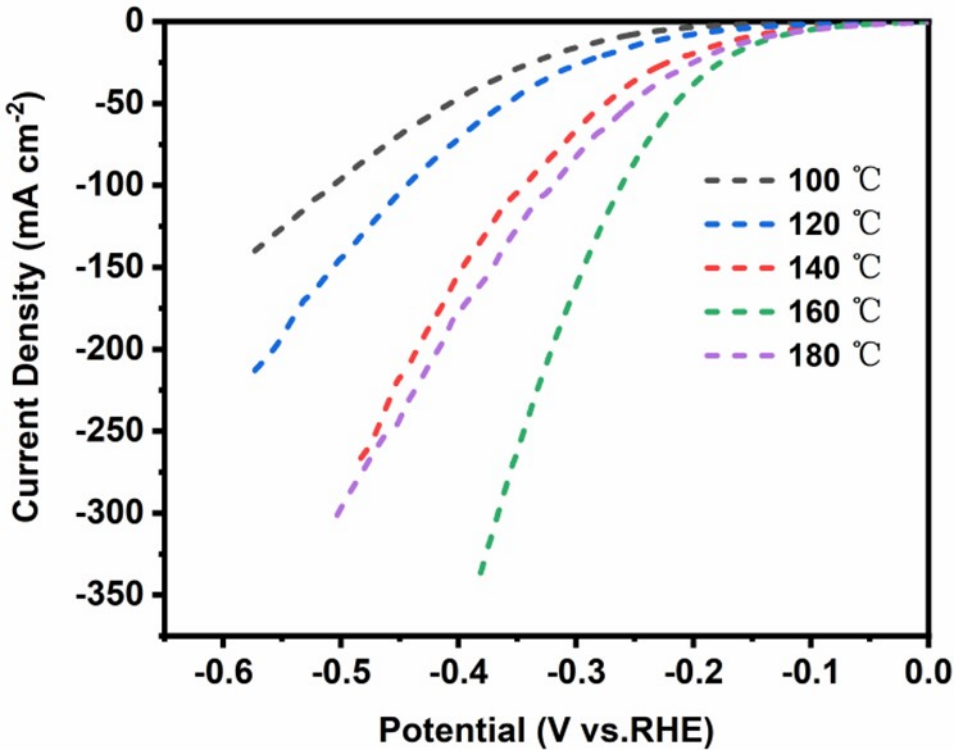


Figure S10. Catalytic activities of $Ni_2Co_1$ LDH-$CeO_x$/$Ni_3S_2$@NF prepared at different hydrothermal temperatures (100-180℃) in 1 M KOH.

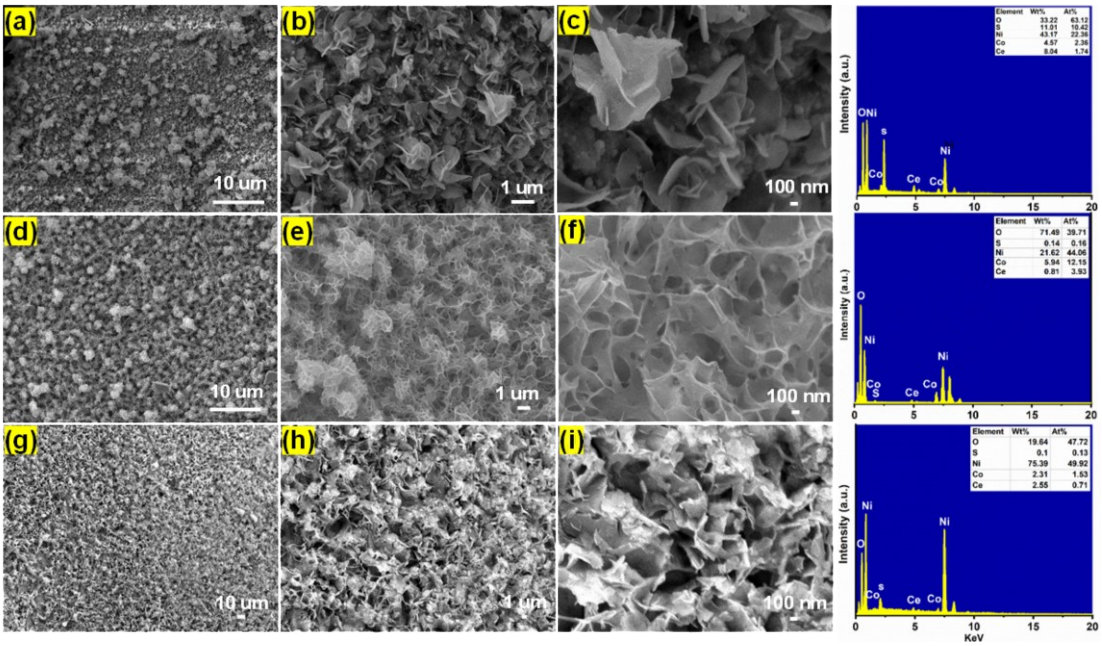


Figure S11. SEM images of $Ni_mCo_n$ LDH-$CeO_x$/$Ni_3S_2$@NF with Ni and Co molar ratios of (a-c) 1:1, (d-f) 1:2, and (g-i) 4:1 at different magnifications and their corresponding EDS results.

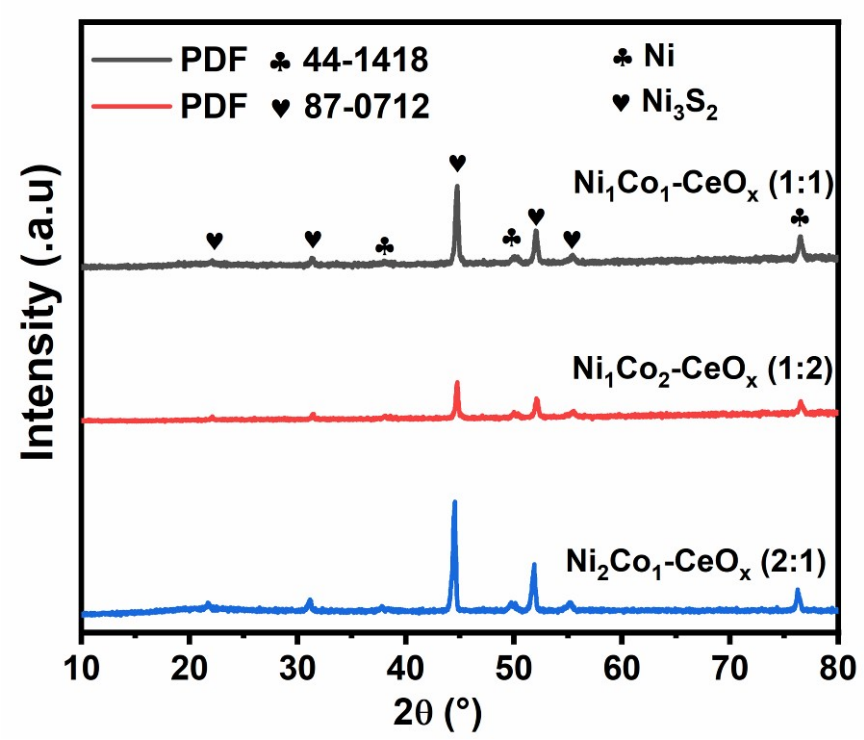


Figure S12. XRD patterns of $Ni_mCo_n$ LDH-$CeO_x$/$Ni_3S_2$@NF with different molar ratios (Ni and Co).

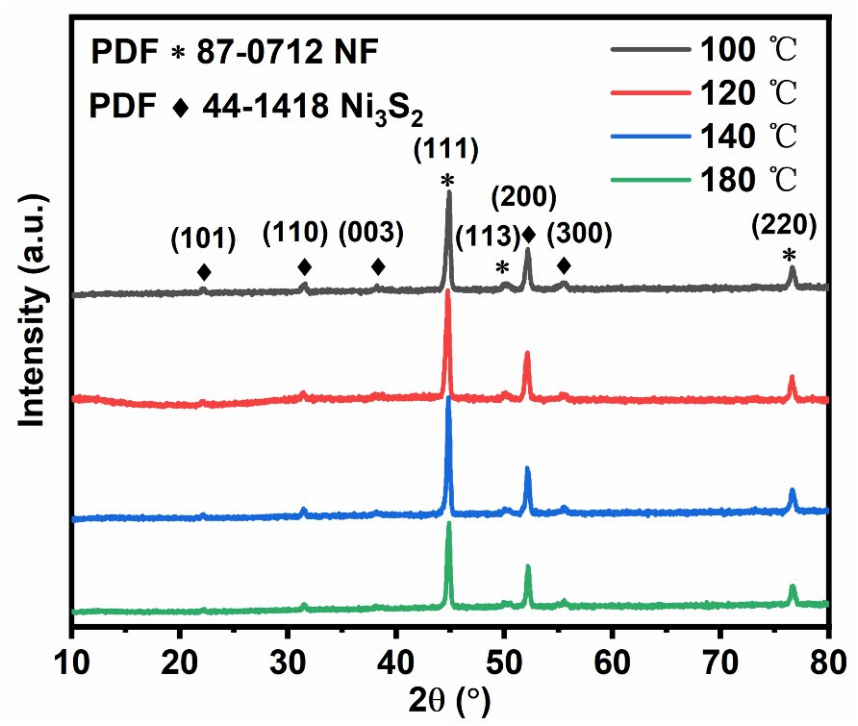


Figure S13. XRD patterns of $Ni_2Co_1$ LDH-$CeO_x$/$Ni_3S_2$@NF at different hydrothermal temperatures (100-180 ℃).

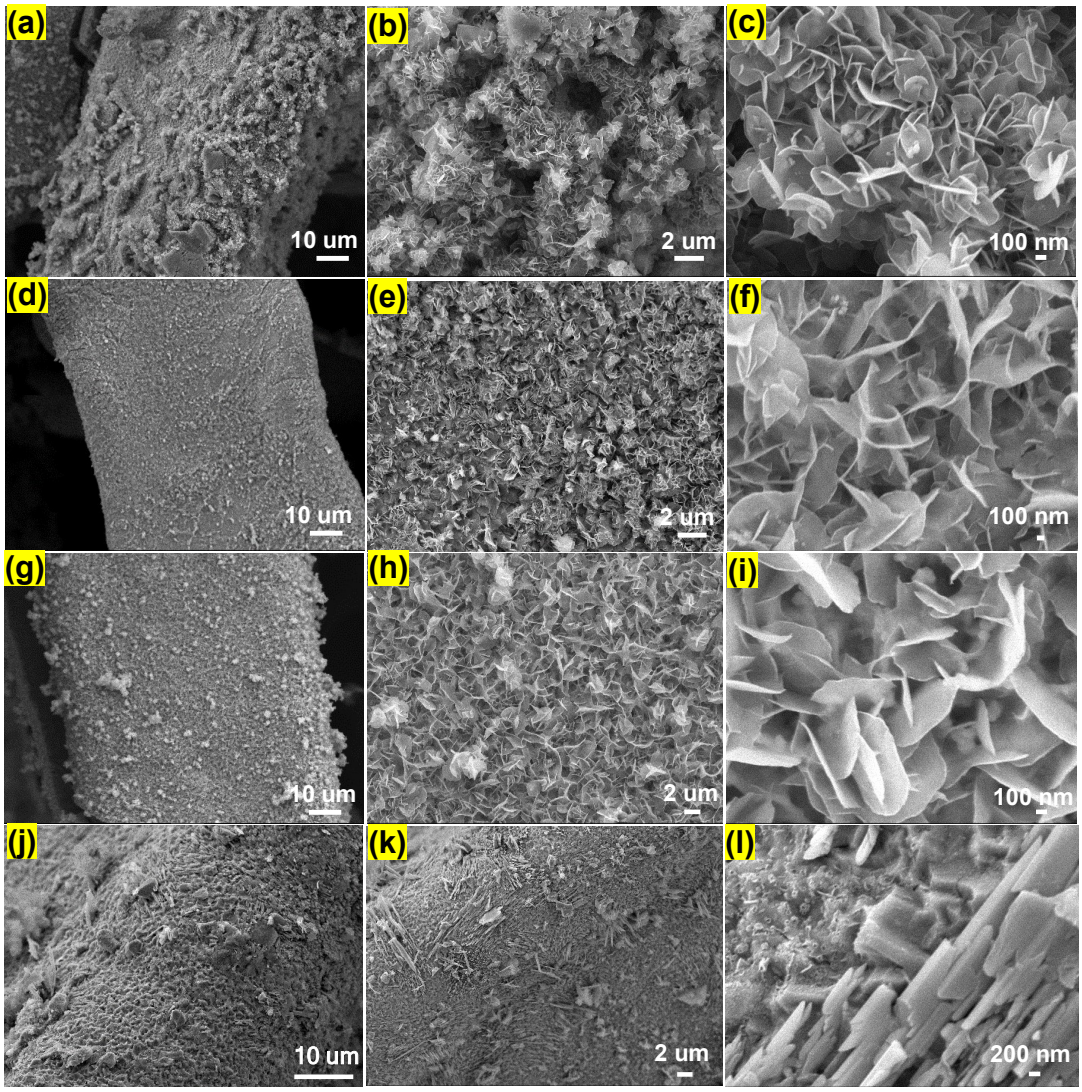


Figure S14. SEM images of $Ni_2Co_1$ LDH-$CeO_x$/$Ni_3S_2$@NF at (a-c) 100℃, (d-f) 120 ℃, (g-i) 140℃, and (j-l) 180℃ hydrothermal temperature.

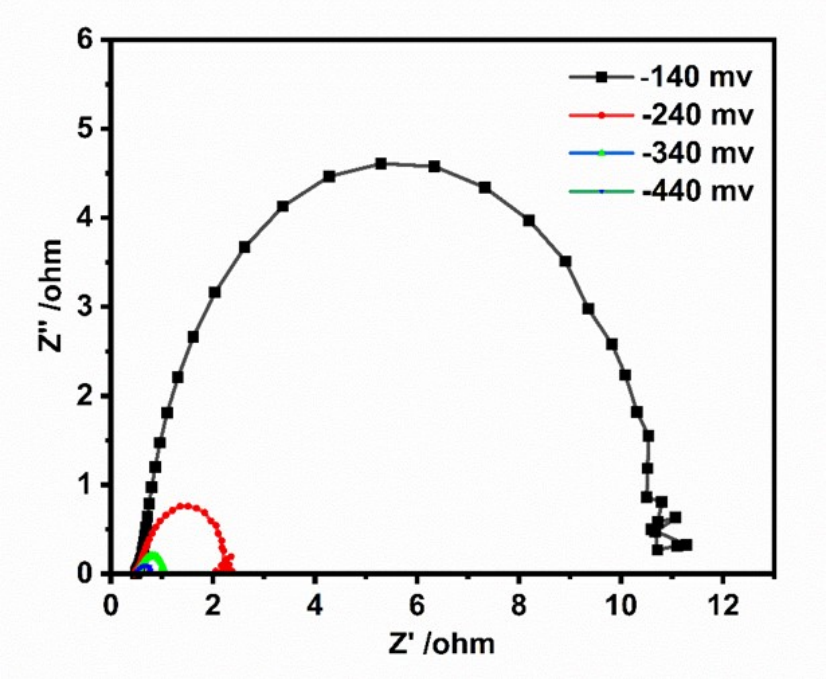


Figure S15. Electrochemical impedance spectra (EIS) of the $Ni_2Co_1$ LDH-$CeO_x/Ni_3S_2$@NF electrode measured with overpotentials from -140 to -440 mV.

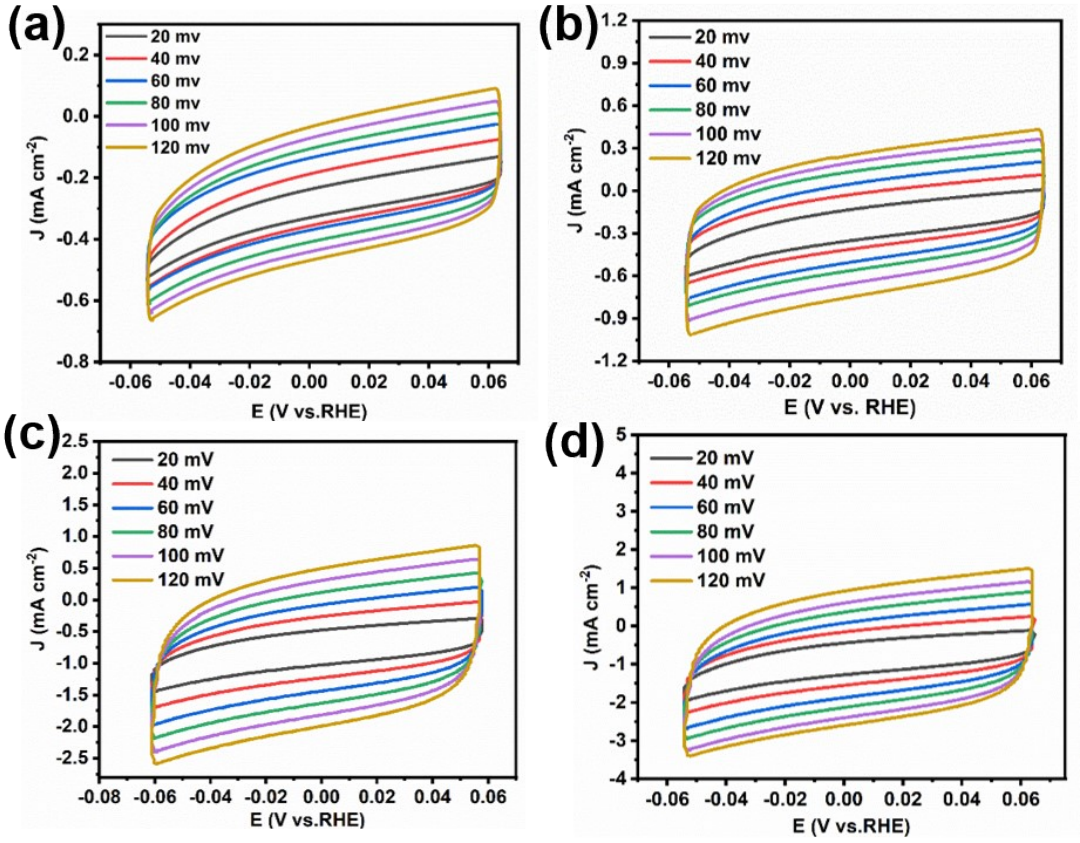


Figure S16. CV curves of (a) NF, (b) $Ni_3S_2$@NF, (c) $Ni_2Co_1$ LDH/$Ni_3S_2$@NF, (d) $Ni_2Co_1$ LDH-$CeO_x$/$Ni_3S_2$@NF in the non-Faradaic capacitance at varying scan rates (20-120 $mV \cdot s^{-1}$) in 1 M KOH.

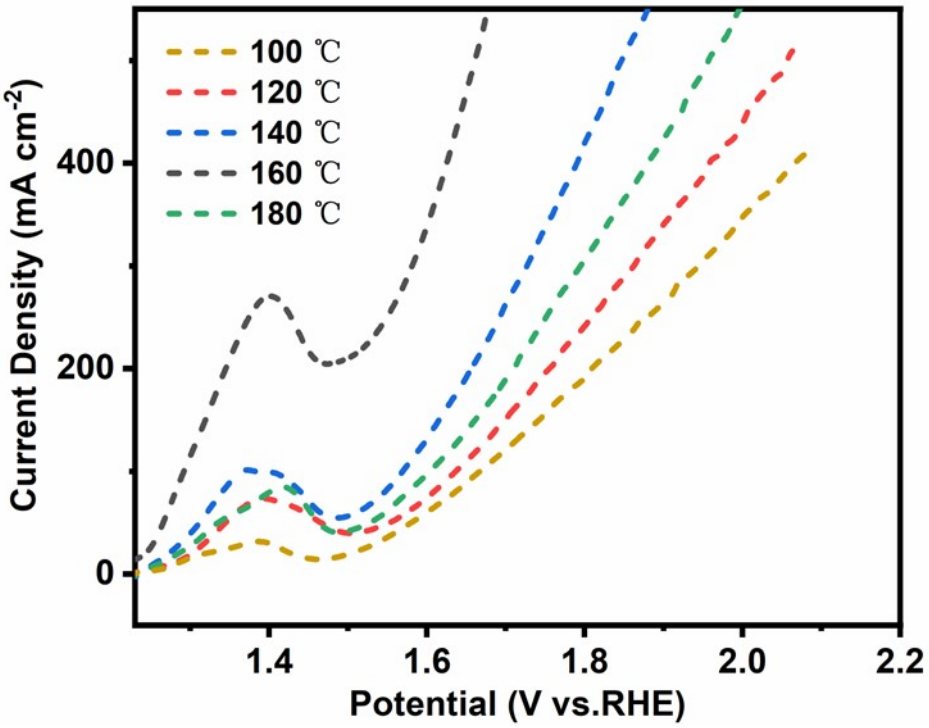


Figure S17. Catalytic activities of $Ni_2Co_1$ LDH-$CeO_x$/$Ni_3S_2$@NF at different hydrothermal temperatures (100-180 ℃) in 1 M KOH.

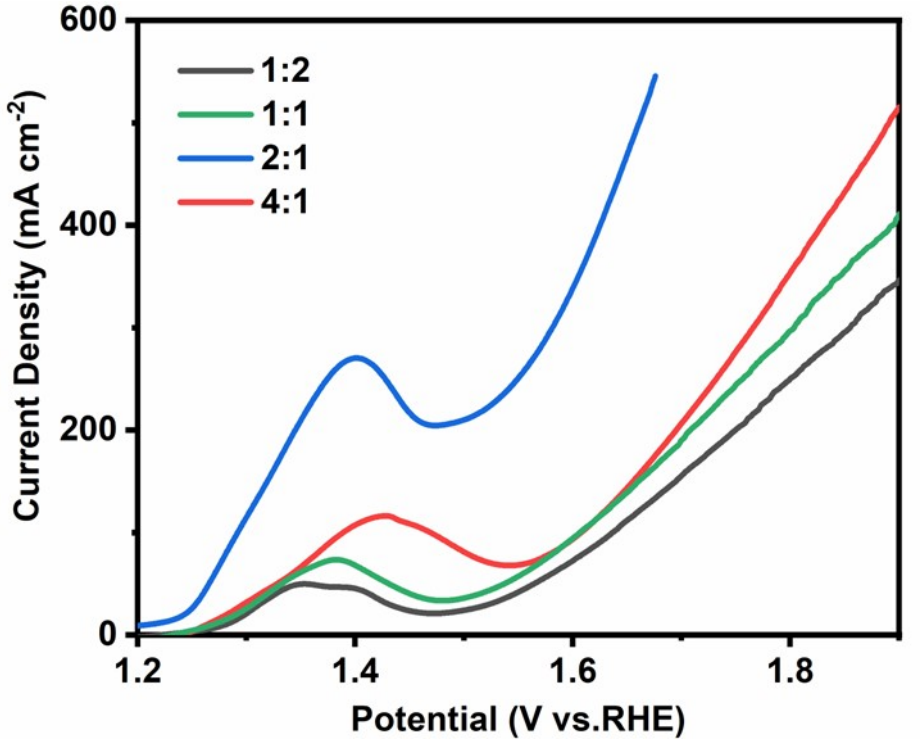


Figure S18. LSV curves of $Ni_mCo_n$ LDH-$CeO_x$/$Ni_3S_2$@NF at different Ni/Co ratios for OER in 1 M KOH.

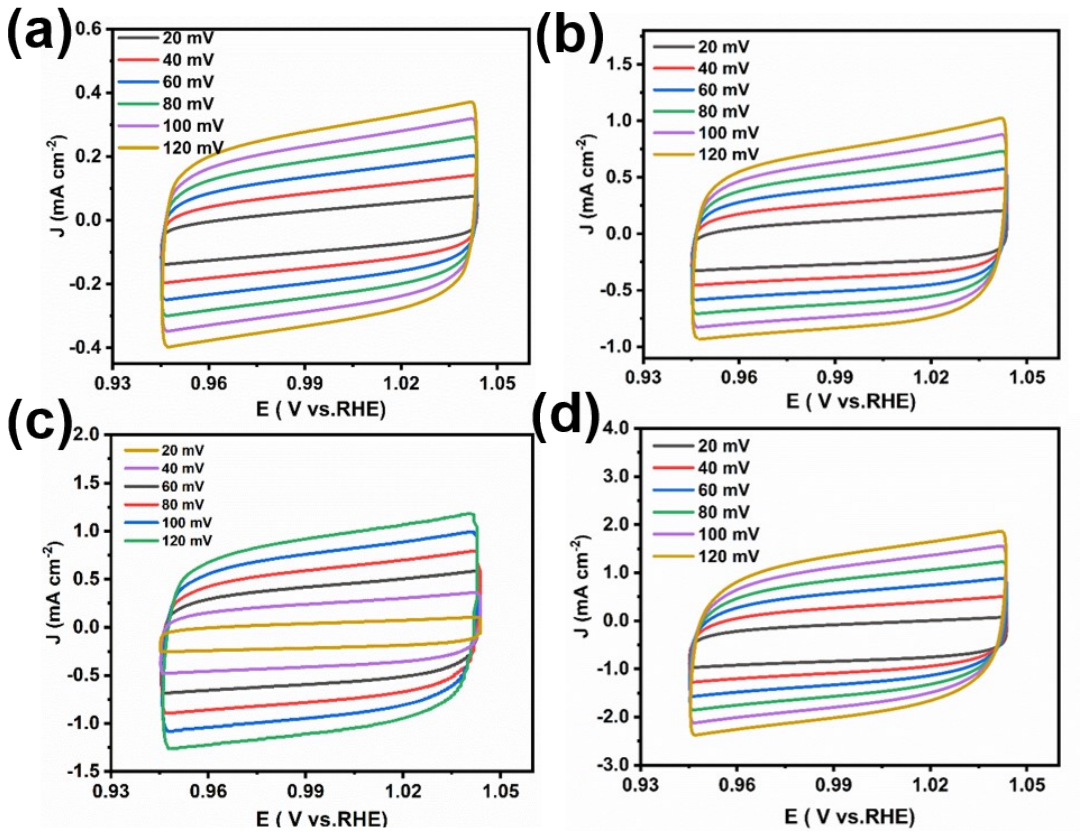


Figure S19. CV curves of (a) NF, (b) $Ni_3S_2$@NF, (c) $Ni_2Co_1$ LDH/$Ni_3S_2$@NF, (d) $Ni_2Co_1$ LDH-$CeO_x$/$Ni_3S_2$@NF in the non-Faradaic capacitance at varying scan rates (20-120 $mV \cdot s^{-1}$) in 1 M KOH.

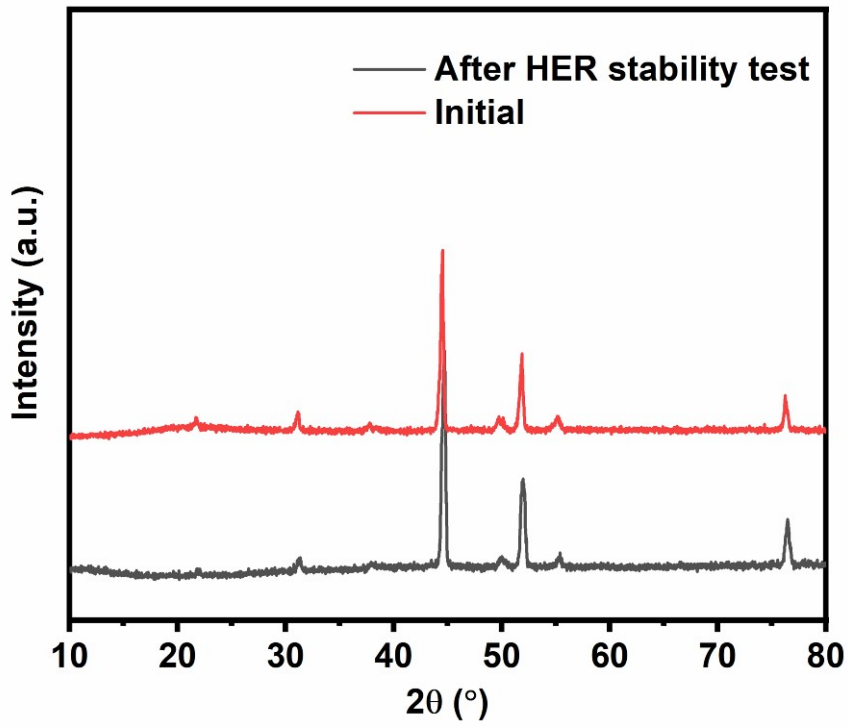


Figure S20. XRD pattern of $Ni_2Co_1$ LDH-$CeO_x$/$Ni_3S_2$@NF before and after 50 h HER stability test.

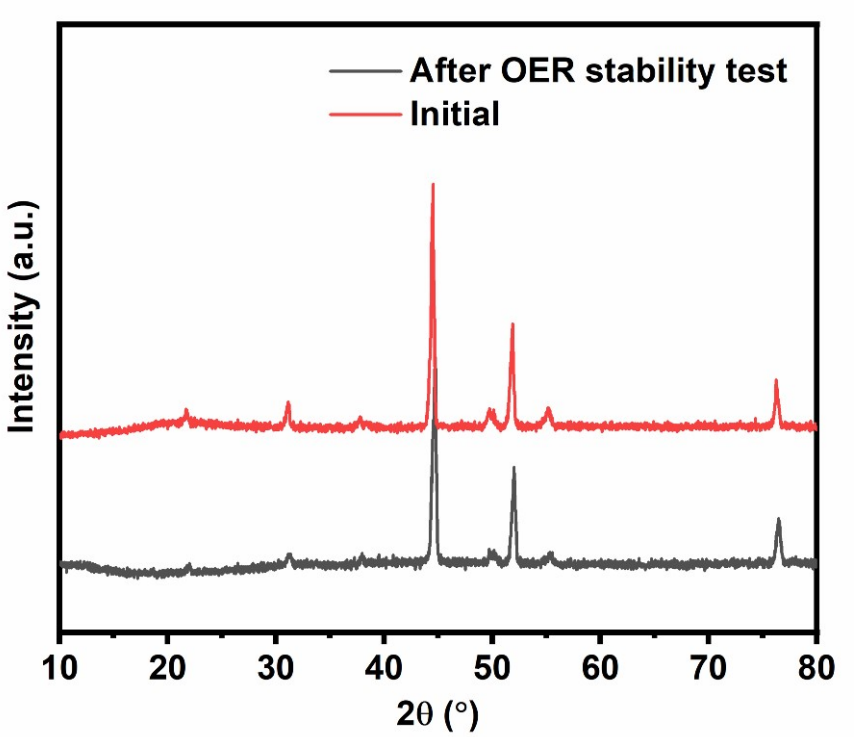


Figure S21. XRD pattern of $Ni_2Co_1$ LDH-$CeO_x$/$Ni_3S_2$@NF before and after 50 h OER stability test.

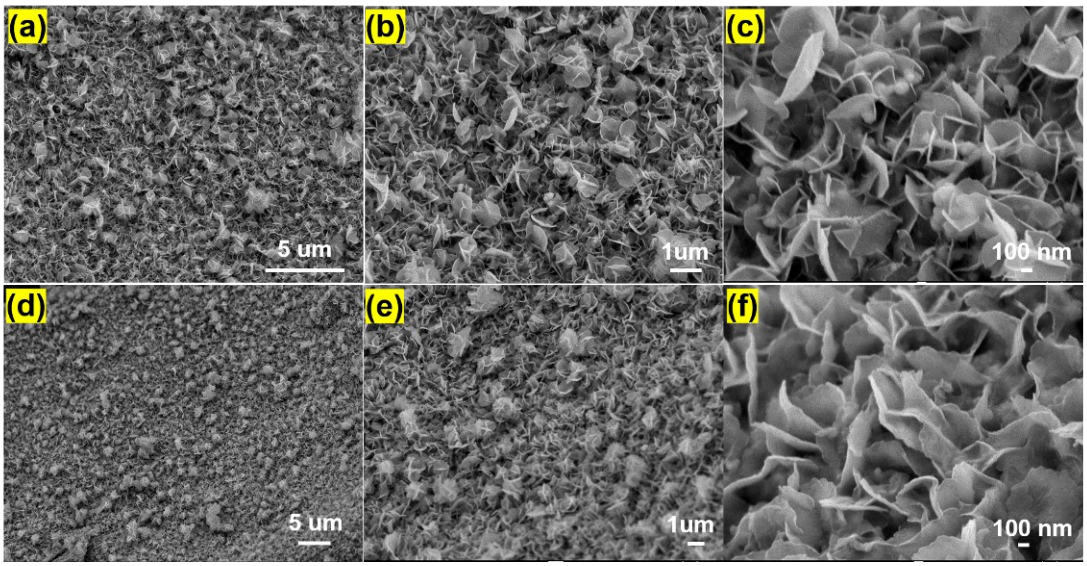


Figure S22. SEM images of $Ni_2Co_1$ LDH-$CeO_x$/$Ni_3S_2$@NF after (a-c) HER and (d-f) OER stability test at different magnifications.

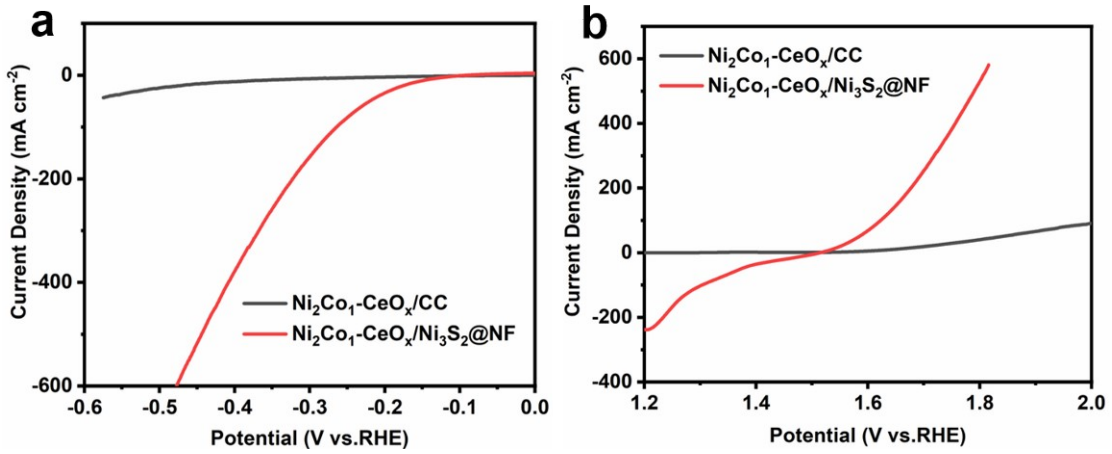


Figure S23. LSV curves of the $Ni_2Co_1$ LDH-$CeO_x$@CC and $Ni_2Co_1$ LDH-$CeO_x$/$Ni_3S_2$@CC for (a) HER and (b) OER in 1 M KOH solution.

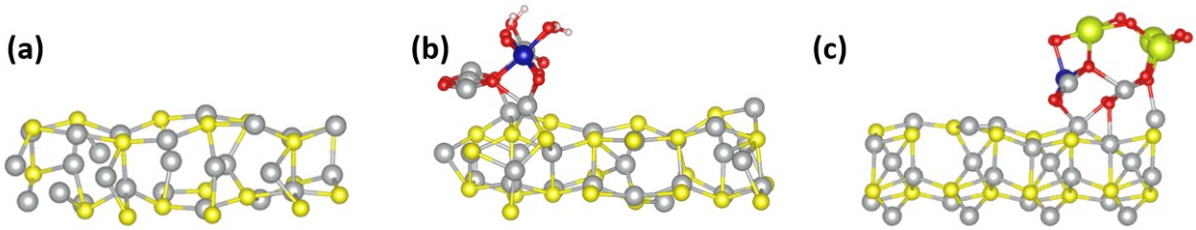


Figure S24. Computational models for (a) $Ni_3S_2$ (110), (b) $Ni_2Co_1$ LDH/$Ni_3S_2$@NF and (c) $Ni_2Co_1$ LDH-$CeO_x$/$Ni_3S_2$@NF. The grey, yellow, green, red, blue, and white balls represnt Ni, S, Ce, O, Co, and H atoms, respectively.

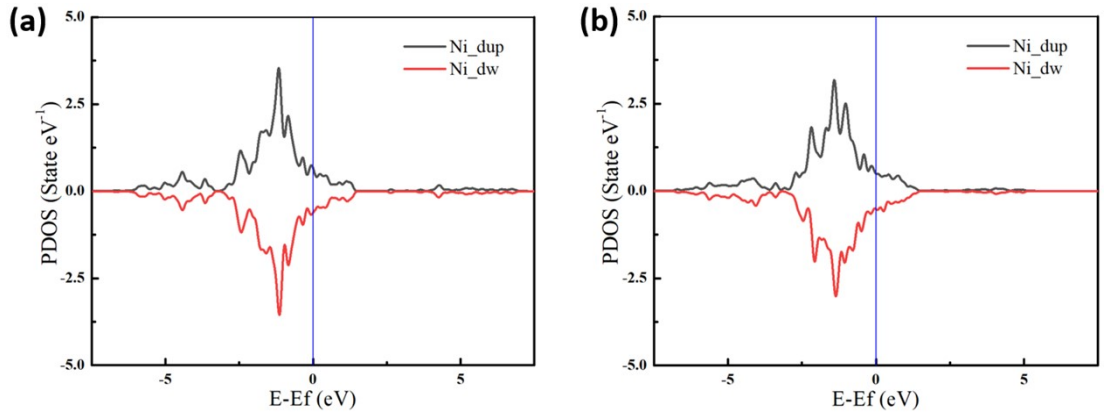


Figure S25. Calculated DOS profiles for signle surface Ni on (a) $Ni_2Co_1$ LDH/$Ni_3S_2$@NF and (b) $Ni_2Co_1$ LDH-$CeO_x$/$Ni_3S_2$@NF.

Table S1. Comparison of the activity of HER and OER with the as-reported transition metal-based sulfide electrocatalysts for water splitting in 1 M KOH.

| **Electrocatalysts** | **η for HER @corresponding j (mV@mA cm$^{-2}$)** | **η for OER @corresponding j (mV@mA cm$^{-2}$)** | **stability of water splitting (V or mA cm$^{-2}$@h)** | **Scan rate (mVs$^{-1}$)** | **Ref.** |
|---|---|---|---|---|---|
| **$Ni_2Co_1$LDH-$CeO_x$/$Ni_3S_2$@NF** | **265@100** | **310@100** | **100 mA cm$^{-2}$@50** | **5** | **This work** |
| $Ni_3S_2$ @G@$Co_9S_8$ | NA | 350@100 | 100 mA cm$^{-2}$@50 | 5 | [3] |
| $Ni_3S_2$ /Cu–NiCo@NF | 304@100 | 218@100 | 100 mA cm$^{-2}$@12 | 5 | [4] |
| Ni–$Ni_3S_2$ | 57@10 | 295@20 | 10 mA cm$^{-2}$@30 | 5 | [5] |
| $Ni(OH)_2$/$Ni_3S_2$/NF | 319@100 | 185@100 | 100 mA cm$^{-2}$@100 | 5 | [6] |
| $Co_3O_4$@$Ni_3S_2$/NF | NA | 260@20 | 10 mA cm$^{-2}$@12 | 5 | [7] |
| $CoS_x$/$Ni_3S_2$@NF | 204@10 | 280@20 | 370mV@10 | 5 | [8] |
| CoNi LDH-$Ni_3S_2$/NF | 193@100 | 382@100 | 10 mA cm$^{-2}$@22 | 5 | [9] |
| $Co(OH)_2$/$Ni(OH)_2$ | NA | 270@20 | 20 mA cm$^{-2}$@24 | 5 | [10] |
| Ce-NiCo–LDHs | 134@50 | 250@50 | 17 mA cm$^{-2}$@48 | 5 | [11] |
| CoS/NiS/NF | 210@10 | 145@10 | 10mA cm$^{-2}$@10 | 5 | [12] |
| CoS NF/CC | 247@50 | 310@10 | 100 mA cm$^{-2}$@20 | 5 | [13] |
| $Ni_3S_2$-$CoMoS_x$/NF | 234@10 | 90@10 | 10 mA cm$^{-2}$@65 | 5 | [14] |
| $Ni_3S_2$@NGCLs/NF | 134@10 | 271@10 | 10 mA cm$^{-2}$@40 | 5 | [15] |
| NF-$Ni_3S_2$/$MnO_2$ | 102@10 | 260@10 | 100 mA cm$^{-2}$@36 | 5 | [16] |
| CoNi-OH\|S@NF | 167@10 | 270@10 | 50 mA cm$^{-2}$@12 | 5 | [17] |
| MnCo@NiS | NA | 286@10 | 50 mA cm$^{-2}$@20 | 5 | [18] |
| $NiS_2$ NWs/CFP | 165@10 | 246@10 | 30 mA cm$^{-2}$@20 | 5 | [19] |

**Table S2** Calculated free energy G for OER intermediate states (OH*, O*, OOH*) with an applied potential U=0 V, in unit of eV. Clean catalyst has been shown as *.

| Reaction step | $Ni_2Co_1$ LDH/$Ni_3S_2$@NF | $Ni_2Co_1$ LDH-$CeO_x$/$Ni_3S_2$@NF |
|---|---|---|
| $* + H_2O \rightarrow OH* + (H^+ + e^-)$ | 1.80 | 1.64 |
| $OH* \rightarrow O* + (H^+ + e^-)$ | 2.74 | 2.13 |
| $O* + H_2O \rightarrow OOH* + (H^+ + e^-)$ | 3.78 | 3.56 |
| $OOH* \rightarrow O_2(g) + * + (H^+ + e^-)$ | 4.92 | 4.92 |

**Table S3** Calculated free energy change ΔG for OER intermediate states (OH*, O*, OOH*) with an applied potential U=1.23 V, in unit of eV.

| Reaction step | $Ni_2Co_1$ LDH/$Ni_3S_2$@NF | $Ni_2Co_1$ LDH-$CeO_x$/$Ni_3S_2$@NF |
|---|---|---|
| $* + H_2O \rightarrow OH* + (H^+ + e^-)$ | 0.57 | 0.41 |
| $OH* \rightarrow O* + (H^+ + e^-)$ | 0.28 | -0.33 |
| $O* + H_2O \rightarrow OOH* + (H^+ + e^-)$ | 0.09 | -0.13 |
| $OOH* \rightarrow O_2(g) + * + (H^+ + e^-)$ | 0 | 0 |

**Reference**

[1] Y. Zhu, W. Zhou, Y. Chen, J. Yu, M. Liu, Z. Shao, *Adv. Mater.*, 2015, **27**, 7150-7155.

[2] C. McCrory, S. Jung, J. Peters, T. Jaramillo, *J. Am. Chem. Soc.*, 2013, **135**, 6977-16987.

[3] Q. Dong, Y. Zhang, Z. Dai, P. Wang, M. Zhao, J. Shao, W. Huang, X. Dong, *Nano Research*, 2018, **11**, 1389-1398.

[4] L. Jia, G. Du, D. Han, Y. Hao, W. Zhao, Y. Fan, Q. Su, S. Ding, B. Xu, *J. Mater. Chem. A*, 2021, **9**, 27639-27650.

[5] L. Jia, G. Du, D. Han, Y. Hao, W. Zhao, Y. Fan, Q. Su, S. Ding, B. Xu, *Advanced Energy and Sustainability Research*, 2021, **2**, 2100078.

[6] J. Li, L. Jiang, S. He, L. Wei, R.-F. Zhou, J. Zhang, D.S. Yuan, S. Jiang, *Energy Fuel.*, 2019, **33**, 12052-12062.

[7] Y. Gong, Z. Xu, H. Pan, Y. Lin, Z. Yang, X. Du, *J. Mater. Chem. A*, 2018, **6**, 5098-5106.

[8] S. Shit, S. Chhetri, W. Jang, N.C. Murmu, H. Koo, P. Samanta, T. Kuila, *ACS Appl. Mater. Interfaces* 2018, **10**, 27712-27722.

[9] Y. Liu, Y. Zhao, Y. Zhang, S. Xing, *Electroanal.* 2023, **35**, e202200251.

[10] L.-F. Gu, C.-F. Li, J.-W. Zhao, L.-J. Xie, J.-Q. Wu, Q. Ren, G.-R. Li, *J. Mater. Chem. A*, 2021, **9**, 13279-13287.

[11] H. N. Dhandapani, D. Mahendiran, A. Karmakar, P. Devi, S. Nagappan, R. Madhu, K. Bera, P. Murugan, B.R. Babu, S. Kundu, J. Mater. Chem. A, 2022, **10**, 17488-17500.

[12] R. Guo, S. Zhang, H. Wen, Z. Ni, Y. He, T. Yu, J. You, New J. Chem., 2021, **45**, 1887-1892.

[13] Y. Li, X. Fu, W. Zhu, J. Gong, J. Sun, D. Zhang, J. Wang, *Inorg. Chem. Front.*, 2019, **6**, 2090-2095.

[14] L. Zhao, H. Ge, G. Zhang, F. Wang, G. Li, *Electrochim. Acta*, 2021, **387**, 138538.

[15] B. Li, Z. Li, Q. Pang, J.Z. Zhang, *Chemi. Eng. J.*, 2020, **401**, 126045.

[16] Y. Xiong, L. Xu, C. Jin, Q. Sun, *Appl. Catal. B: Environ.*, 2019, **254**, 329-338.

[17] Y. Yan, K. Bao, T. Liu, J. Cao, J. Feng, J. Qi, *Chemi. Eng. J.* 2020, **401**, 126092.

[18] X. Wang, L. Li, L. Xu, Z. Wang, Z. Wu, Z. Liu, P. Yang, *J. Power Sources*, 2021, **489**, 229525.

[19] Y. Guo, D. Guo, F. Ye, K. Wang, Z. Shi, *Int. J. Hydrogen Energy*, 2017, **42**, 17038-17048.